Hindawi
Modelling and Simulation in Engineering
Volume 2024, Article ID 1769145, 15 pages
https://doi.org/10.1155/2024/1769145

Research Article

Maximizing Electric Power Recovery through Advanced Compensation with MPPT Algorithms

Souad Touairi, Mustapha Zekraoui, and Mustapha Mabrouki

Industrial Engineering and Surface Engineering Laboratory, Faculty of Sciences and Techniques, Sultan Moulay Slimane University, Beni Mellal, Morocco

Correspondence should be addressed to Souad Touairi; touairisouad@gmail.com

Received 9 August 2023; Revised 31 January 2024; Accepted 14 February 2024; Published 7 March 2024

Academic Editor: Dimitrios E. Manolakos

The present investigation introduces an advanced methodology for maximum power point tracking (MPPT) applied to a piezo harvester scheme. A comprehensive rectifier circuit, equipped with an embedded MPPT component, is established to optimize energy production by monitoring a DC-DC inverter connected to the rectifier. Furthermore, the system's sensitivity error has been finely tuned to dynamically adjust its impedance unit in real time, thereby optimizing load acquisition. This innovative approach seamlessly integrates the MPPT algorithm into the piezo harvester circuit. Moreover, the vehicle's road handling is significantly augmented through the incorporation of a robust steering front and an active differential control system. Leveraging the MPPT module, the rectifier consistently achieves a power recovery efficiency exceeding 85%, independent of varying load conditions. Additionally, a DC-DC converter circuit has been seamlessly integrated to finely adjust the output voltage to meet specified levels. Numerical simulations demonstrate the effectiveness of the harvesting scheme, extracting a substantial output power of 90 W with an overall efficiency of 70%. The improved MPPT approach, employing angles of arrival (AoA) DV-Hop control strategies, minimizes the system's power consumption based on the Global Positioning System (GPS). The utilization of Harris Hawks optimization (HHO) and the generation of quadrants in the four-quadrant operation mode of DC motors in the wireless sensor network (RCSFs) have been significantly enhanced in this study. Simulations reveal that, at a velocity of 50 km/h, shock absorbers utilizing the received signal strength indication (RSSI) can harvest between 60 and 90 W on a class C road, based on the time of arrival (TOA). Striking a balance in ride comfort using the time difference of arrival (TDOA) as a trade-off constitutes approximately 30% of the piezoelectric harvester (PEH) system's power consumption when operating in active suspension mode, optimized by particle swarm optimization (PSO).

1. Introduction

In premium electric vehicles, the imperative of extended range is becoming increasingly critical as the integration of a greater number of components aims to improve comfort performance levels. To accommodate concerns about ride quality, increasing emphasis is being applied to the adoption of electronically controlled suspension (ECS) systems, comprising both semiactive and fully active systems with increasing capabilities, in electric vehicles [1]. Over recent decades, considerable research has been devoted to addressing the problems associated with energy autonomy, in particular, the powering of embedded sensors [2]. Even though integrated sensors have been gaining in accuracy, reliability, and robustness while reducing their size, the limited lifetime of their power supply is a major drawback [3]. One promising approach is to harness ambient mechanical energy to ensure sustainable power autonomy [4]. Minimizing the energy consumption of electronic components has substantially contributed to the progress of wireless mobile applications [5]. Conversely, however, batteries, which initially powered the growth of portable electronic devices, are now hampering further progress due to associated maintenance issues, such as recharging and replacement [6]. Although the performance of electric vehicle parts and subsystems improved substantially between 2003 and 2024, as demonstrated by the logarithmic scale [7], battery development has revealed its limitations [8]. In addition, scientists

have highlighted the fact that battery technology is not evolving as dynamically as other electric vehicles. In this regard, researchers have emphasized that battery efficiency advances more gradually than other technological developments [9].

In this context, energy efficiency is not expected to grow rapidly over time and seems to be approaching a certain degree of saturation [10]. This development brings up the subject of alternative energy resources [11]. The studies of authors [12, 13] provide a summary of the various potential energy supplies. Several solutions have been envisaged, based on the concept of traditional batteries, i.e., based on energy reservoirs [14]. Firstly, there are fuel cells, which are the subject of much current research [15]. Nevertheless, these batteries are still expensive, difficult to miniaturize, and pose problems for the hydrogen storage [16]. A more radical solution consists in using nuclear batteries [17], for which energy densities are thousands of times higher than those of lithium-ion chemical batteries. The authors of [18] have developed batteries using low-energy radioisotopes whose radiation does not penetrate more than a few tens of micrometers through most solid or liquid bodies [19]. These batteries are perfectly harmless since radioactive radiation cannot pass through (or infiltrate) simple plastic packaging [20]. However, their major setbacks lie in the collection and reprocessing of used batteries [21]. In 1995, researchers listed the progress of logic and memory functions since the 1970s [22]. Their work concentrated on advancements in metal-oxide-semiconductor (MOS) technology, a pivotal semiconductor technology extensively employed in the manufacturing of integrated circuits (ICs) and microelectronics. The innovations in MOS technology have enabled the reduction of power consumption in chips while simultaneously enhancing the efficiency of logic and memory functions [23]. On the other hand, the concept of a wireless sensor network allows remote monitoring and data processing [24]. This latter, related to complex and distributed automobiles, has been able to substantially develop, thanks to these technical advances [25]. The authors of [26] summarized the progress made to limit the electrical consumption of such networks in the automotive industry. These developments dealt with both the actual physics of the components used and the solicitation strategy of the nodes within the overall architecture of the network [27]. In [28], the researchers noted that current progress on the energy consumption of on-board devices in modern vehicles made it possible to consider other power resources resulting from the ambient energy exploitation. This has enabled getting rid of battery toxicity and short lifetimes' drawbacks that hugely impact wireless sensor networks [5]. Indeed, in the case of networks made up of a very large number of nodes, replacing all the batteries is difficult to consider [29]. In [30], the authors focused on powering a wireless sensor network node from the surrounding vibrational energy. It showed the power density evolution as a function of a lifetime for batteries, solar, and vibration resources [31]. The power densities are given in microwatt per cubic centimeter, except in the case of solar energy where it is given in microwatt per square centimeter [32]. There is not a function of time, unlike the energy density of batteries [33]. In other words, the suspension quality greatly contributes to the car's handling and braking for driving pleasure and safety [34]. This latter keeps the vehicle well insulated from road disturbances (such as bumps) and within an acceptable steering limit [35]. Moreover, road disturbances and loads are considered two main factors affecting the vehicle comfort [36]. For this issue, road roughness is considered as a small value at high frequency, whereas a hill is considered a larger value at the low frequency of road discomfort [37]. Vibratory energy recovery is aimed then at realizing microelectrical generators of centimetric size allowing electronic system feed by absorbing the "ambient" energy present in the surrounding environment [38–40]. Typically, the vehicle's suspension system consists of a spring and dampers—-which are used for the vehicle's adaptive oscillation, linking the vehicle to its wheels [41]. A promising application for communication sensors is the MPPT controller of vehicle harvestable energy [42]. These autonomous networks' development responds to a growing need to measure, analyze, and control our natural environment's evolution, the behavior of civil or military constructions, or the state of our human body health [43]. Suspension system's performance has recently been improved due to the sustainable increase in vehicle efficiency [44]. Several suspension system design proposals have been introduced to increase the vehicle suspension system performance and sophistication by redefining the element boundaries [45]. A large number of simulation experiments have been executed in the Simulink 2021a environment in order to investigate the performance of the suggested MPPT control [46].

The MPPT based on the maximum area method for the PV system operating under rapid variation of solar irradiation has been provided [47]. Recently, significant attention has been paid to photovoltaic pumping systems based on maximum power point monitoring by the sine cosine optimization algorithm [48]. To produce maximum power from the photovoltaic system for various climatic conditions, an Artificial Bee Colony (ABC) method was implemented and compared with two other perturbation and observation (P&O) MPPTs [49]. In order to improve the tracking performance of the MPP controller for optimal system energy extraction under partial shading conditions (PSC), a fast and accurate algorithm for global maximum power point tracking (GMPP) based on the sine-cosine algorithm (SCA) has been presented [50]. Additionally, a Thevenin source-resistance representation commonly used solar system model is simplified into [51]. Furthermore, the authors in [51] introduced a control algorithm, known as the proposed maximum power point tracking (MPPT) algorithm.

This work's main purpose was implemented through an effective design of a hybrid maximum power point tracking (MPPT) for assessing ride comfort, power consumption, and potential energy harvesting under road irregularities generated according to the ISO standard. The established scheme is based on linear tangents-interpolation (LT-I) techniques. The latter has been applied to an energy harvesting system bonded to an active suspension of a quarter car model based on adaptive fuzzy and active force control (AF-AFC).

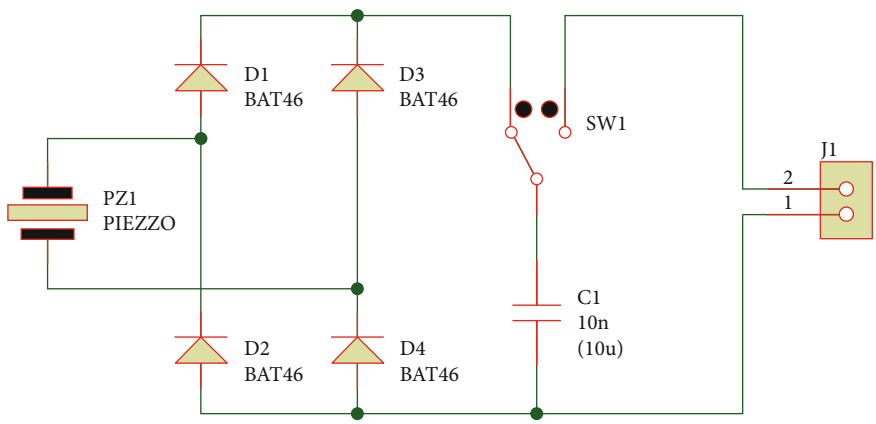

Figure 1: *PVEH* model connected to the DC-DC converter.

Furthermore, the energy recovery system has been evaluated based on the following criteria: spring-mass acceleration, spring-mass displacement, suspension deflection, and tire acceleration which are known to significantly influence the ride comfort performance of the vehicle. The proposed LT-I scheme's performance has been compared with perturb and observe (P&O) and advanced divide and conquer (DC) algorithms.

By incorporating the suggested system into the quarter-car suspension, it is indeed possible to improve the overall performance in the relevant frequency range (0-100 Hz). This enhancement is achieved by improving the skyhook control benefit and using a lower passive damping coefficient than that applied in a conventional suspension assembly.

The structure of this paper is described as follows: in Section 2, a maximum power point tracking (MPPT) has been presented as a controller model implemented on the piezoelectric voltage output, using the Harris Hawks optimization algorithm. Section 3 provided an introduction to the bond graph (BG) model. Next, Section 4 detailed the active flutter (AF) and active fault tolerance (AFC) mechanisms, focusing on the combined BG AF and AFC scheme. Section 5 dealt with the simulation procedure and presented the results. Section 6 concluded with a synthesis of the main results.

2. MPPT Controller Applied to Piezoelectric Voltage Output Using Harris Hawks Optimization Algorithm

2.1. The Electrochemical Parameters of the Proposed PEH. A lot of methods have been reported to enhance the energy obtained by reverting or inverting the integrated capacitor once the interior current supply passes over zero [2, 5]. Though the reviewed systems achieve improved extreme power extraction, the output load resistance range for achieving high power extraction is good. However, when the system load is beyond this defined range, the productivity level rises significantly. Thus, the traditional complete-bridge rectifier is exposed in Figure 1.

The electrical characteristics of piezoelectric generators are generally very favorable: AC and high voltage, low current, and capacitive output impedance. Therefore, the energy produced by these piezoelectric generators is generally not directly usable for the supply of conventional electronic devices which require a low-voltage DC supply. As a rule, a rectifier bridge followed by a filter capacitor is used to convert the AC voltage delivered by the piezoelectric inserts into DC voltage. With a sinusoidal mechanical load of constant amplitude, it can be shown that there is an optimum load resistance at which the power output of the piezoelectric inserts is maximum. A DC-DC converter is often inserted between the rectified voltage and the load to be supplied (see Figure 1). This converter can have several roles: either to impose a constant voltage on the load (voltage regulation) or to impose a V_{rec}/I_{rec} ratio equal to the optimal resistance to optimize the power supplied by the microgenerator (impedance matching).

2.2. Proposed Rectifier and MPPT Controller for the Power Recovery Process. This section highlights an MPPT scheme that has been extensively used in dynamic systems. The purpose of the analysis is to provide an overview of the different power ranges of this harvester: describing their operating principles and highlighting their advantages and limitations. This will be useful for the reader who needs a comprehensive education on power harvesting methods, as well as to keep abreast of the latest developments in this field. From there, the ultimate goal of this strategy is to research the power gap in the proposed system. This gap will be the basis of the research that will be conducted in this work.

Figure 2 illustrates the established MPPT approach for a piezo energy recovery scheme. This device is attached to the complete-bridge circuit to convert the AC output voltage of the piezo into a DC signal. In addition, a DC-DC circuit tracks the equipment to adjust V. The DC-DC transformer regulated the generated signal using the proposed MPPT controller. This enhanced MPPT energy controller tracks the system's threshold setpoint and then regulates the DC-DC mode of operation. Furthermore, the rectifier output followed the MPPT output voltage to maximize the voltage value V, when the harvested voltage of the rectifier is adjusted to V_{ref}. The output voltage may be higher or lower than V_{ref}. The bucket-boost model is adapted to be used for

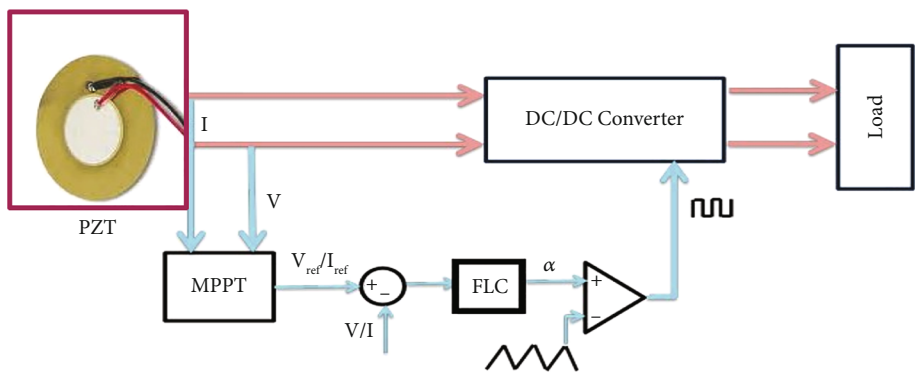

Figure 2: *MPPT* model connected to PVEH converter.

DC-DC conversion. The proposed MPPT method is based on the duty cycle control of the DC/DC convertor.

The basic idea behind MPPT is to find and operate the power generation system (such as optimum current and voltage) at its maximum power point, where it can generate the maximum amount of electrical energy. The power generated by these systems is influenced by various factors, including vibration intensity, temperature, and vehicle speed, all of which can change dynamically, but these factors are not always the same.

Connecting high-voltage current directly with low-voltage current may impact the charging efficiency of the capacitor to some extent; for this, the FLC has been used in this case of studies.

Currently, the primary approach to mitigate the connection loss between high- and low-voltage currents involves employing distinct boost circuit and step-down circuit modules based on the MPPT connected to an FLC block. Therefore, Table 1 describes PVEH recuperator rules implemented in a fuzzy logic controller to control and optimize the operation of an energy recuperator, in order to maximize the energy recovery efficiency and regulate the recovered output power, to ensure the implementation of a broadband ambient vibration energy recovery system.

This processing ensures that the voltage difference between the two currents remains within a reasonable range, thereby minimizing the impact of their connection on the charging efficiency of the capacitor including perturb and observe (P&O), incremental conductance, and various heuristic algorithms. These algorithms use different strategies to track and adjust the operating point based on the characteristics of the power generation system. This particular type is described as the direct MPPT control approach; the controller equation system is extracted and verified by the bond graph inverse (BGI) model. The fuzzy logic control (FLC) block is employed, and the duty cycle is directly calculated by the controller. Consequently, it delivers the MPPT scheme with optimally simplified control while keeping the maximum results [31]. The high performance of the existing control made it possible to use bond graph modeling (BGM) in the MPPT controller. By using BGM, the observability of the system is not mandatory. This is a key advantage because operating point changes, nonlinearities, and uncertainties such as unmodeled physical quantities can be handled excellently. Nevertheless, the automotive designer must have prior knowledge of how the power output responds qualitatively to the inputs. With the use of a complete band gap rectifier, the AC transducer signal is converted to a DC mode signal. As the excitation frequency of the PEH header is small (inferior to 100 Hz), the activated diodes could be operated by a transmitter and a detector. To decrease the amount of energy wasted through the rectifier, all corrector devices are configured as dynamic diodes to achieve a minor voltage drop. By switching to the activated junction rectifier, the dropped potential in the individual diode is decreased from 400 mV to 10 mV.

Table 1: FLC rules connected to PVEH scavenger.

	Vpzt				
Vch	NB	NS	ZO	PS	PB
NB	ZO	ZO	PB	PB	PB
NS	ZO	ZO	PS	PS	PS
ZO	NS	ZO	ZO	ZO	PS
PS	NS	NS	NS	ZO	ZO
PB	NB	NB	NB	ZO	ZO

2.3. Harris Hawks Optimization Algorithm. Harris Hawks optimization approach is a bioinspired algorithm based on the cooperative search behavior of Harris Hawks. The process involves the integration of various tools, such as social rules and communication strategies, to guide the search for an optimal solution. The optimization problem involves identifying the optimal solution for a given function by adjusting its variables, typically confined to a specific range of values. This constraint may lead to a subconstrained optimization problem. Mathematically, the goal is to minimize the function F over the set E, meaning to find a value ε within E such that [5]

$$F(x^*) = \min\ (\text{ou}\ \max) f(x). \tag{1}$$

During the exploration phase in the Harris Hawks optimization (HHO) algorithm, sharks land randomly in different locations and wait to detect prey using two strategies:

```
Inputs: Population size N and maximum number of iterations T
Outputs: Rabbit location and fitness value Initialize random population X(i = 1, 2,....., N)
As long as (stopping condition not met) do
Calculate vehicle speed values
Set Xrabbit as vehicle location (best location)
End
For (each device( Xi )) do
Update initial energy E0 and displacement force J ►E0=2rand ()-1, J=2(1-rand ())
Update E using Eq. (3)
If (|E| ≥ ) then                                        ►Exploration phase
Update the location vector using Eq. (2)
If (|E| < ) then ►Exploration phase
If (r ≥ 0 5 et|E| ≥ 0 5 alors)                          ► gentle siege
Update the location vector using Eq. (5)
If no if (r ≥ 0 5 et|E| < 0 5 ) then                    ► Soft seat with fast Progressive dives (6)
If not if (r < 0 5 et|E| ≥ 0 5 ) then                   ► Gentle siege with progressive fast dives updates the location vector using . . (Eq (5))
If not if (r < 0 5 et|E| < 0 5 ) then ►Hard seating with progressive fast dives updates the location vector using (Eq (6))
Return Xrabit
End.
```

Algorithm 1: Optimization algorithm by Harris Hawks.

$$X(t+1) = \begin{cases} X_{\text{rand}}(t) - r_1|X_{\text{rand}}(t) - 2r_2X(t)|, & 0,5 \le q, \\ (X_{\text{rabit}}(t) - X_m(t)) - r_3(\text{LB} + r_4(\text{UB} - \text{LB})), & q \le 0.5, \end{cases} \tag{2}$$

where $X(t+1)$ represents the position vector of the road irregularities at the next iteration $t+1$, $X_{\text{rabit}}(t)$ denotes the position of the speed bump, and $X(t)$ is the current position vector of the bridges. The variables r_1, r_2, r_3, r_4, and q are random numbers within a specified interval [0,1], updated at each iteration. LB and UB indicate the upper and lower bounds of the variables, $X_{\text{rand}}(t)$ signifies a randomly selected device from the current population, and $X_m(t)$ denotes the average position of the current population of devices. The average position of the maximum power is attained using Equation (2).

$$X_m(t) = \frac{1}{N}\sum_{i=0}^{N} X_i(t), \tag{3}$$

where $X_i(t)$ indicates the position of each device at iteration t and N represents the total number of devices.

To model exploration to operation, the energy consumed by the vehicle is modeled as follows:

$$E = 2E_0\left(1 - \frac{t}{T}\right). \tag{4}$$

And E indicates the harvester energy of the piezoelectric, T is the maximum number of iterations, and is E_0 is the initial state of its energy.

$$X(t+1) = \Delta X(t) - E|jX_{\text{rabit}}(t) - X(t)|, \tag{5}$$

$$\Delta X(t) = X_{\text{rabit}}(t) - X(t). \tag{6}$$

3. Modeling and Optimization of the Piezoelectric Harvester

3.1. Modeling and Control of Vehicle Motion Dynamics for Energy Harvesting. In this modeling, some mechanical energy is calculated for several reasons, including estimating the inequality of energy requirements. The energy flow in a piezoelectric energy recuperator in a schematic diagram is modeled by the following equations:

$$\begin{aligned} i_{\text{pzt}} &= \frac{1}{t_{\text{pz}}}\left[\int_{t_1}^{t_{\text{pz}}} \text{I}_{\text{pz}} \sin(\text{wt})dt - \frac{V_{\text{rec}} + 2V_D}{R_{\text{pz}}}\left(t_{\text{pz}} - t_1\right)\right] \\ &= \frac{1}{t_{\text{pz}}}\left[I_{\text{pz}}\frac{\cos(wt_1) - \cos\left(wt_{\text{pz}}\right)}{w} - \frac{V_{\text{rec}} + 2V_D}{R_{\text{pz}}}\left(t_{\text{pz}} - t_1\right)\right]. \end{aligned} \tag{7}$$

To estimate the collected energy, the average power output i_{pzt} is first determined. In which Ip and ω are the input current amperage and angular velocity frequency i_{pzt}, respectively. The power collected by the continuous wave bridge rectifier is as follows:

$$P_{\text{pzt}} = \frac{V_{\text{rec}}}{t_{\text{pz}}}\left[I_{\text{pz}}\frac{\cos(wt_1) - \cos\left(wt_{\text{pz}}\right)}{w} - \frac{V_{\text{rec}} + 2V_D}{R_{\text{pz}}}\left(t_{\text{pz}} - t_1\right)\right]. \tag{8}$$

The greatest amount of power collected by the entire wavelength bridge circuit is achieved once:

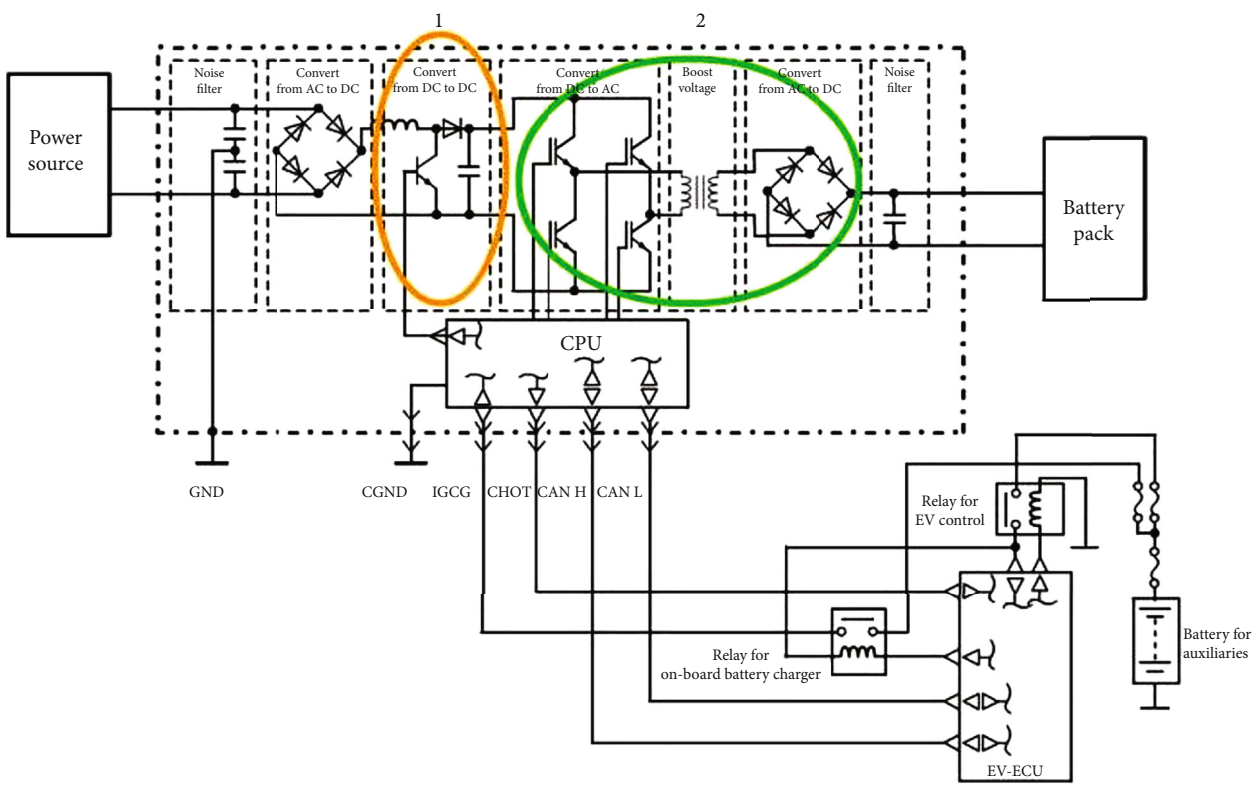

Figure 3: *DC-DC* model connected to PVEH scavenger.

$$V_{\text{rec}} = \frac{I_{\text{pzt}}}{2wC_{\text{pzt}}} - V_D. \tag{9}$$

The output power P_{out} and extreme output power $P_{\max}$ are specified by Equation (2) through the hypothesis that the power drop inside an individually dynamic diode is zero. While most fuzzy logic controllers previously evolved have been of the rule-based type, in which the controller's simple rules attempted to provide a model of the controller's reaction to particular process statuses, traditional fuzzy logic control implied four different operation components or methodology for fuzzification, property function, fuzzy inference procedure, and defuzzification process [10]. According to [13], an adaptive fuzzy logic system that uses a Takagi-Sugeno scheme is briefly discussed in this section. It integrates a generally applied computational back-propagation learning approach in a neural network scheme. The adaptive fuzzy model is applied to the MPPT controller as illustrated in Figure 3. In this system, the framework will be established in the normal initialization process and all fuzzy belonging functions are attached to create a full class of rules. The system consists of a fuzzy product inference engine, a singleton fuzzifier, a central mean, and a Gaussian membership function.

$$\begin{aligned} \{\varepsilon_{\text{pzt}}\} &= [K_i]\{\delta_i\} - [M_i]\{E_i^2\}, \\ \{D_{\text{pzt}}\} &= [e_i]\{\delta_i\} + [g_i]\{E_i^2\}. \end{aligned} \tag{10}$$

In the following formula, $\{D_{\text{pzt}}\}$ and $\{\varepsilon_{\text{pzt}}\}$ denote the deformation and constraint tensors. K_i and e_i are the resilience, pseudo-piezoelectric coupling, and permittivity dielectric constants, correspondingly. The harvester electromechanical stress layer has been obtained by applying Hamilton's approach. Because of the inverse and primary piezoelectric natural frequency, an electromechanical constraint between the electrical and mechanical stress can be calculated using the AFC model. In the statement sequence listed here, $\{E_i^2\}$ refers to the electric movement matrix. $[e]$ indicates the matrix of the dielectric rigidity and is the deflection vector. $\{g\}$ is the matrix of dielectric magnitude. $\{\text{Ep}\}$ is the vector of electric flow, $[\sigma]$ is the stress vehicle, and $[C]$ is the resilient substance for a typical electric flow field:

$$[M_{\text{rec}}] * \{V_{\text{outp}}\} + [V_{\text{rec}}] * \{V_{\text{pzt}}\} + [K_{\text{pzt}}] * \{V_{\text{pzt}}\} = [F_{\text{out}}]. \tag{11}$$

The basic principles of this modern population-based algorithm simulating the hunting behavior of piezoelectric harvester have been explained in this section.

Furthermore, the areas of application of this algorithm and identified its advantages and disadvantages have been investigated. In the next section, we will simulate and adapt this algorithm for the localization of unknown sensors in RCSFs.

3.2. Formulation of Localization Problems. The aim of this work is to identify the location of sensors randomly

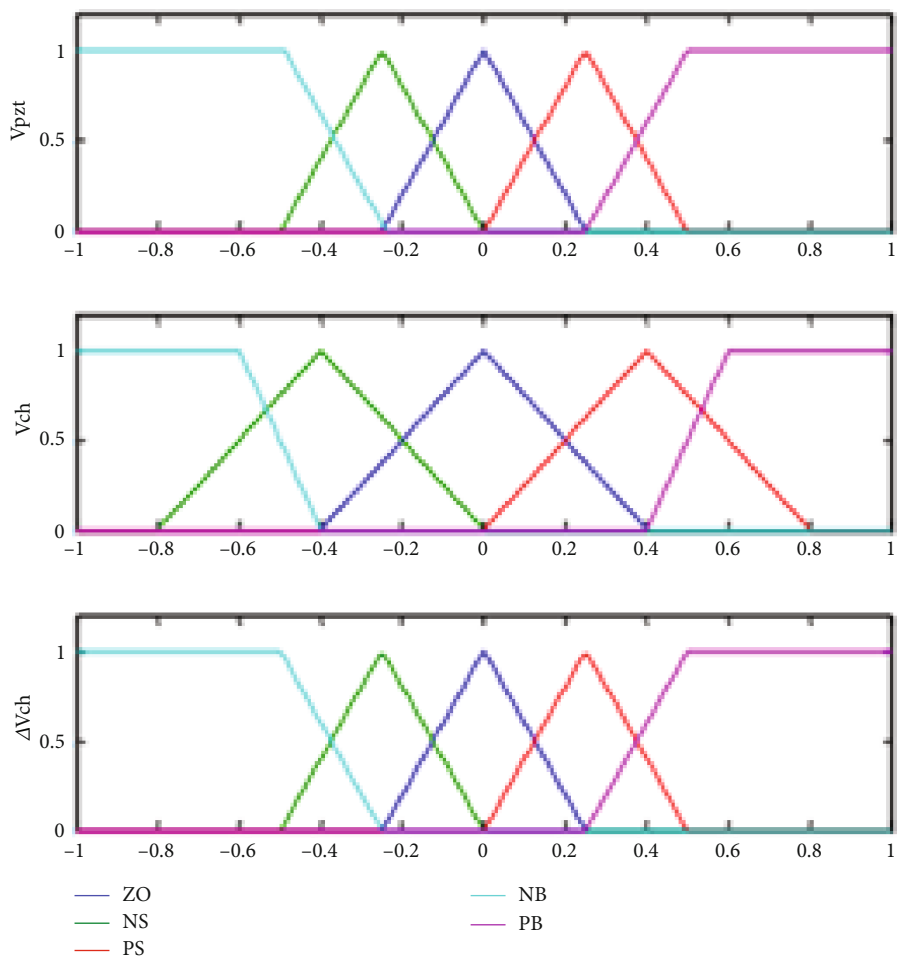

Figure 4: Property features for Vpzt, Vch, and ΔVch of PVEH scavenger.

dispatched in a 2D plane corresponding to the RCS area of interest: for this case, $m \geq 0$ nodes called anchors whose positions are known a priori and have been considered. Moreover, the objective of the localization procedure is to find the positions of n unknown nodes labeled $m+1, \cdots N$ $(N = n + m)$. Each network node is characterized by a similar transmission radius R. Let (x, y) denote the coordinates of the target node and d_i represent the distance between the target node and i^{th} anchor.

The following formula is used to calculate the distance [5]:

$$d_{ij} = \sqrt{\left(x_i - x_j\right)^2 + \left(y_i - y_j\right)^2}. \tag{12}$$

Let $\widehat{d}_i = d_i \mp n$ the distance value obtained from the RSSI method be the error committed when estimating the distance by RSSI. The objective function of the localization problem is determined as follows:

$$F_{(x,y)} = \frac{1}{M}\sum_{j=1}^{M}\left|\widehat{d}_j - d_j\right|. \tag{13}$$

After entering the network parameters, the sensors are randomly deployed in the simulation zone by clicking on the "Deploy" random deployment button (Figures 4 and 5). After entering all the initial network parameters, the parameters of the proposed algorithm (number of iterations and population) must be entered. An example of deployment and localization using the proposed approach is shown in Figure 4. Black squares represent randomly deployed sensors, red diamonds represent anchors, and brown circles indicate anchors. To start the algorithm, click on the "HHO Algo" button. The calculated dummy force of the added skyhook damper is referred to as the transducer load (F_{out}). This latter has been calculated according to the control law of the MPPT controller as

$$[F_{\text{out}}] = \begin{cases} -B_{\text{pzt}} * \xi * z'_u & \text{IF} \quad z_u \leq z_s, \\ -W * \mu * z'_s & \text{IF} \quad z_s \leq z_u, \\ 0 \quad \text{IF} \quad z_s = z_s, \\ M * \delta_{\text{pzt}} * V_{\text{rec}} & \text{IF} \quad z_s = 2 * z_s. \end{cases} \tag{14}$$

A restrained selection of system settings needs to respect the basic requirements of the system, such as

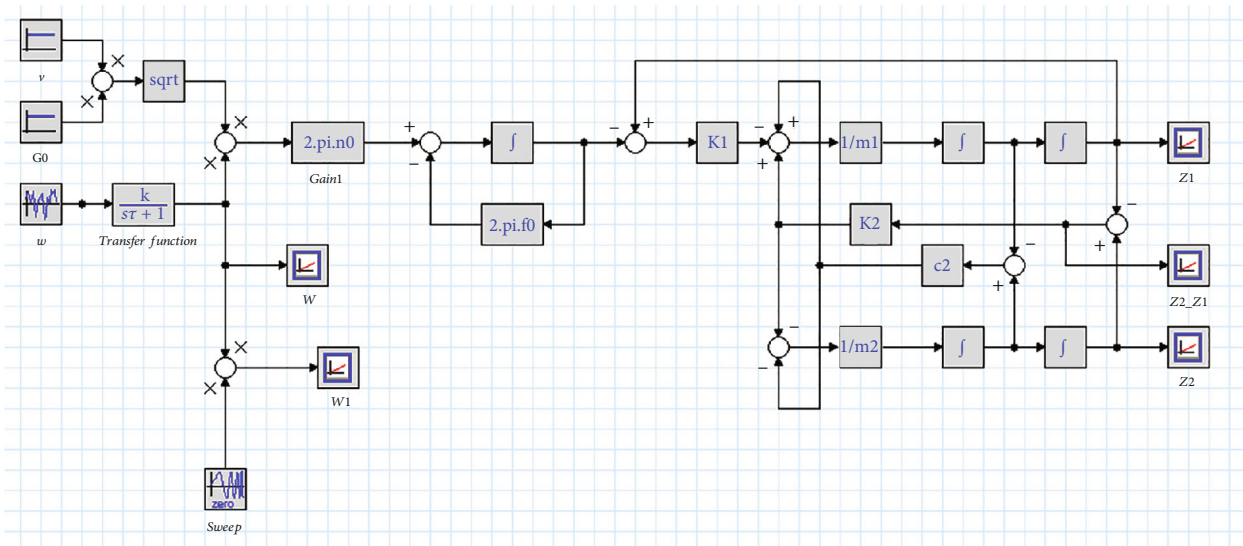

Figure 5: Bond graph phase portrait of MPPT controller for PVEH.

$$0.5 \le \delta_{\text{pzt}} \le 0.9,$$
$$0.05 \le \mu \le 0.2, \tag{15}$$
$$\xi_{\text{pzt}} \le 2.$$

In addition, it is supposed that $\delta_{\text{pzt}} < 0.9$, so that the pendulum weight is less than the support radius for system load, and $\mu < 0.2$ so that the mass of the suspension $m < 0.33$ kg for sensible body weight.

Numerical data that solve the system state equation indicated that the peak occurs between 8 Ω and 10 Ω, confirming that the optimum external load for the coil is between 8 Ω and 10 Ω to achieve maximum output power. The maximum power generated by a single coil is around 0.69 mW.

Following the same principle, the optimum load for the piezoelectric film is between 2 kΩ and 3 kΩ, with maximum output power reaching around 4.55 mW.

The transducer output acquired an AC voltage signal that must eventually be transformed into direct current by an AC-DC converter to be connected to the battery or the ultracapacitor.

$$E_i^p = \left[0\,0\,\frac{1}{t_{\text{pzt}}}\,1\right] \text{ AND } \int_{t_0}^{t_{\text{pzt}}} \left[\left(k - \bar{w} + 2 * \psi - W_{\text{pzt}}\right) * t^{2*\cos(wt)}\right] dt = 0. \tag{16}$$

The optimization approach applied in this section has been classified into two important groups. One is the issue of multiobjective performance; previous research has carried out deep results. The latter is an optimal scheme using GA such as subdivided group optimizer (SGO), artificial beam collection (ABC), divergence element evolution (DE), NSGA-II, and multiobjective unified swarm optimizer with crowding gap (MOUSO-CD).

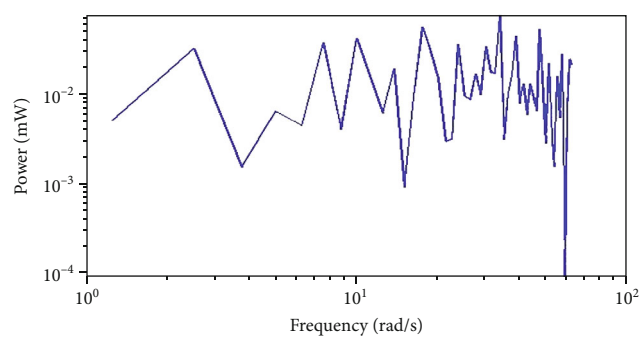

Figure 6: Configuration of the electrical power output in real time.

$$\begin{Bmatrix} \gamma_1 \\ \gamma_2 \\ D_{11} \\ D_{12} \end{Bmatrix} = \begin{bmatrix} k_{11} & k_{12} & 0 & \mu_{14} \\ k_{21} & k_{22} & 0 & \mu_{24} \\ 0 & 0 & k_{33} & 0 \\ \mu_{41} & \mu_{42} & 0 & k_{44} \end{bmatrix} * \begin{Bmatrix} \lambda_1 \\ \lambda_2 \\ \lambda_3 \\ E_4^P \end{Bmatrix} \begin{Bmatrix} \gamma_1 \\ \gamma_2 \\ D_{11} \\ D_{12} \end{Bmatrix}. \tag{17}$$

However, the signal condition in Equation (6) can be changed to a hyperbolic hook form to forestall the control feedback. The harmonic curve provides the global and quadratic stability of the vehicle throughout the movement spectrum of the automobile in modified subsystems (see Figure 1). The ideal initial conditions and forces of the car motion are provided in Equation (5).

3.3. Bond Graph Modeling of the Piezoelectric Harvester. As illustrated in Figure 1, a PZT harvester is conventionally exhibited as a sinusoidal current producer $i_{\text{pzt}}(t) = I_{\text{pzt}} \sin(2\pi f_{\text{pzt}} t)$, parallel to a capacitor C_1.

The amplitude of the PZT current output l_p changed according to the amount of mechanical external excitation of the PZT component; however, it is supposed to be

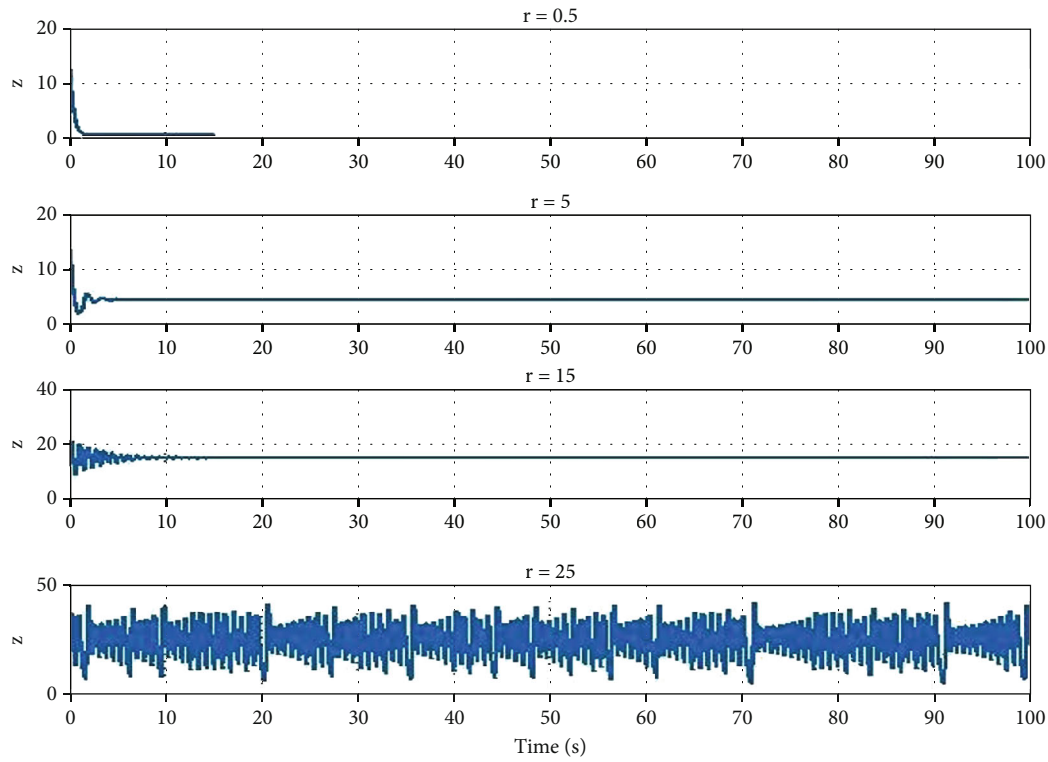

Figure 7: Real vehicle movement according to the road profile.

approximately constant for any external load; γ_{pzt} is the excitation frequency of the PZT element.

4. The AF and AFC Mechanism

The research on the AFC approach was launched by Hewitt and his team in the early 1980s, leading to the design of dynamic control systems. The suggested controller systems could be robust and more stable following enforced perturbations or parametric variations provided that a certain number of criteria are satisfied [14, 15]. The balancing operation of AFC requires the measurement or specification of a certain amount of the measured variables. Therefore, a significant portion of the AFC is designed to be robust and stable with respect to the changes in the variables of interest [16]. Consequently, a lot of mathematical and computational overhead can be considerably decreased, which means that the scheme can be real-time operated. The AFC can be demonstrated to include also Newton's second law of motion's state equations. For an individual active automotive suspension, the equation of motion may be expressed as follows [18]:

$$F_s + Q_s = m_{ss} a_s. \tag{18}$$

F_s is the enforced load, Q_s is the perturbation load, m_{ss} is the hanging mass, and a_s is the acceleration of the suspended mass, accordingly. The AFC diagram has been implemented in the suspension device and piezo harvester system. However, the predicted disturbance value Q' may be of the following form:

$$Q'_s = F'_s - \left(m'_{ss} a'_s\right). \tag{19}$$

The FLC approach is widely considered the most popular choice due to its simplicity [10]. The basic principle of this controller is to induce a disturbance by manipulating the PWM duty cycle commands of the inverters and choppers (either decreasing or increasing them) and then observing its effect on the output piezoelectric collected power (PZH). If the current power $P(k)$ exceeds the previously calculated power $P(K-1)$, the disturbance direction is restored; otherwise, it is reversed. Despite its ease of implementation, the MPPT algorithm is associated with several inherent problems [11].

The primary calculation load in AFC is the propagation of the calculated inertia table with the system dynamical velocity into the AFC prediction loop. The basis of AFC lies (or resides in) employing certain observed and measured values of the individual system properties identified, specifically the detected force and acceleration of the driving system and the projected mass of the system. It is instantly noticeable that the monitoring algorithm used here is extremely easy and has enormous implications in practice since the computational load is very small and it might be readily applied in real time with no problems, as demonstrated by Equation (7). These solution benefits are as follows: (1) the MPPT system design's complexity has been drastically reduced, (2) the

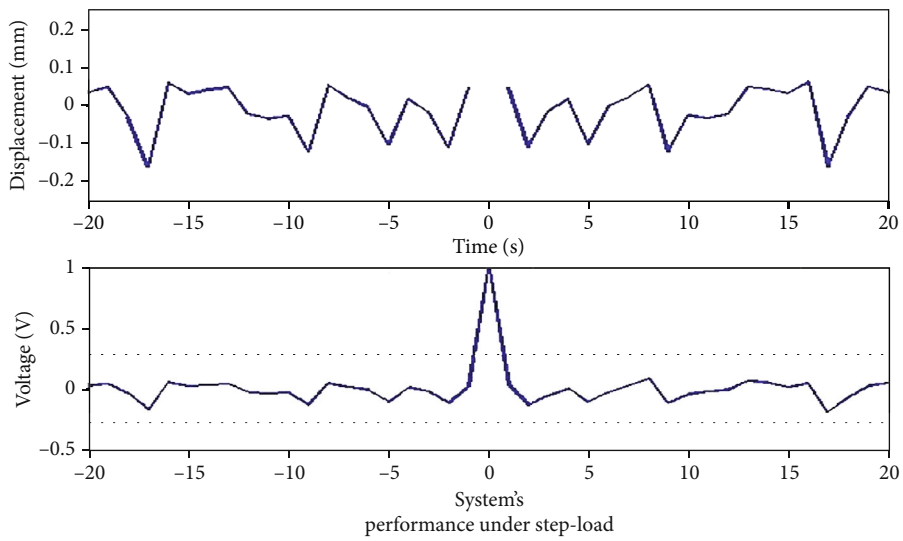

Figure 8: Output voltage produced as a function of the external disturbance.

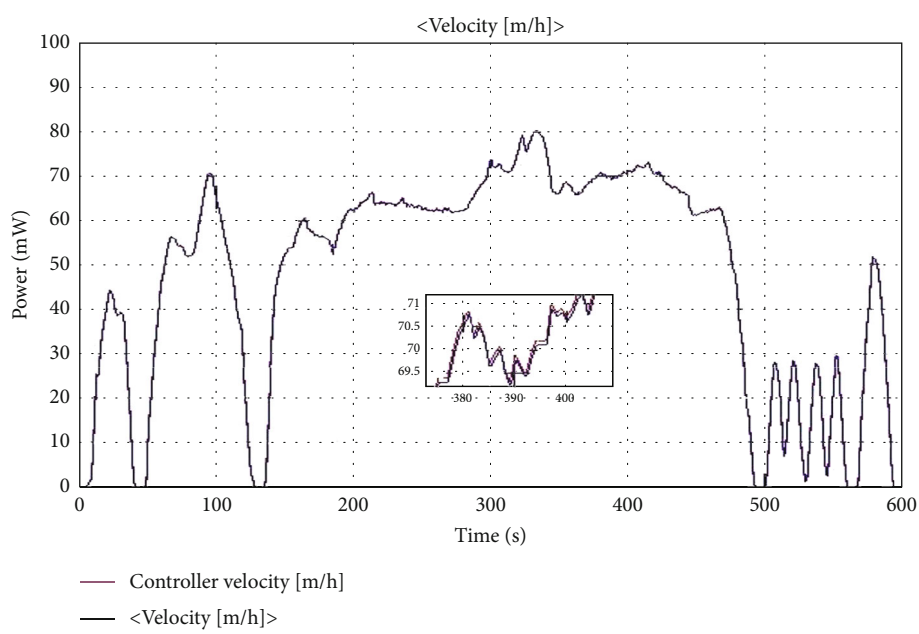

Figure 9: The elevation MPPT rate of electric power for the PVEH.

computation time has been decreased, and (3) no tuning energy was involved for the FL gains.

5. Simulation Outcomes and Experimental Validation

The component proprieties of the quarter car design and the piezoelectric transducer are extracted from [12] which have been in use in the BG model.

The first component of the voltage device of the MPPT controller is the rectifier. With the application of a complete bridge, the circuit has rectified the AC signal from the piezo driver into a DC signal. As a result, all input diodes of the rectifier are implemented as activated diodes to minimize the potential drop. Therefore, the activated natural frequency of the PZT is a low one (less than 1500 Hz). Thus, the dynamic diodes could be realized by a junction transistor and a comparator. By switching to the activated diode, the potential drop in individual diodes is decreased from 400 mV to 10 mV.

Figure 6 depicts the harvester system's output energy with an l0 μF output condenser, and the output potential of the harvester system is near 12 mV. The established PZT energy harvesting schemes provided a (global, total) whole effectiveness of 70%.

The simulation outcomes, illustrated in Figures 7–9, show excellent agreement between the two types of modeling. However, in an open circuit, the average energy flow

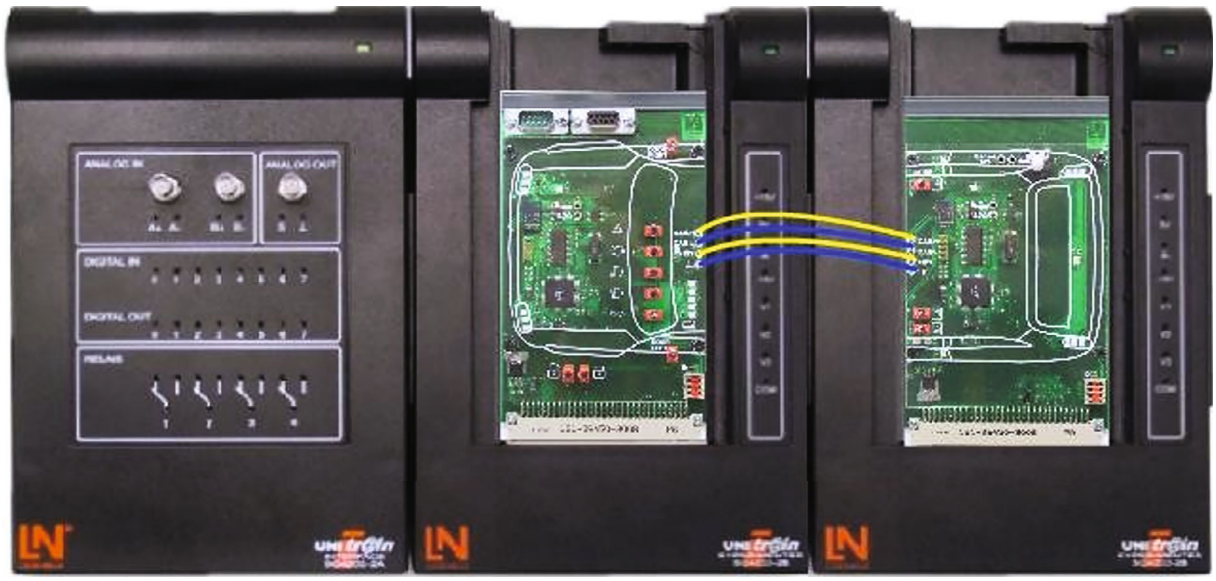

Figure 10: Experimental validation of the proposed piezoelectric energy harvester.

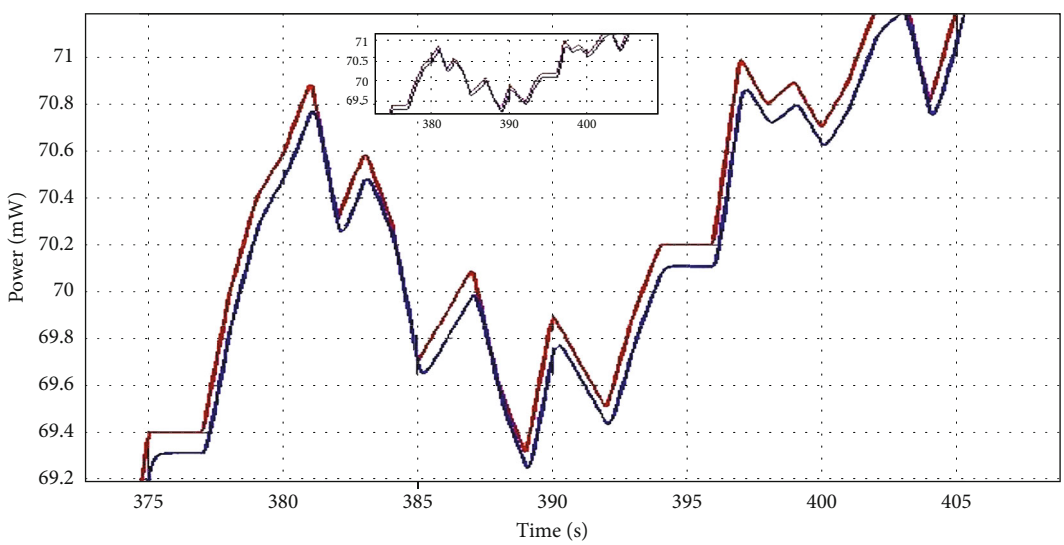

Figure 11: Control of the variation of the power harvested by the PZT according to the sliding surface of the suspension.

between the beam and the piezoelectric patches is not exactly zero for the MATLAB simulation, while it is zero with the localized constant 20-Sim model. This is due to the fact that the piezoelectric elements have intrinsic losses in the ANSYS model but none in the localized constant model where all the viscous losses are taken into account by the global C-damper to the complete structure in the developed BG model. The ANSYS localized constant model is purely monomodal, while the BG model corresponds to the real multimodal structure *C*. Accordingly, Figure 10 illustrates the experimental validation system used in the proposed piezoelectric energy recuperator. The recuperator is implemented in a real system that uses an inverter and a powerful DC-DC chopper to control the energy harvested from a broadband ambient system. To prove and validate the physical phenomena involved in the proposed models, the influence of the geometry of the recuperator on the measured vibratory forces has been modeled. After having instrumented the prototype in Figures 11 and 12 on a traction bench, the damper is connected in series to a BC302 strain gauge sensor as shown in Figure 13. The diagram (HMI) deals with the implication of electrical polarization caused by the application of applied mechanical stress. The test was modified as shown in Figure 14 to vary the rod's position containing the piezoelectric elements with respect to the suspension systems, millimeter by millimeter at very low speeds, i.e., 0.001 m/s. These measurements are carried out in quasistatic mode.

If the system is placed under the conditions of a real road and with the optimal electromechanical values of the recuperator ($f = 23,\ 4\,\text{Hz}$, $R = 220\,\text{k}\Omega$, and amplitude of 400 mVpp) with the addition of the diode bridge followed

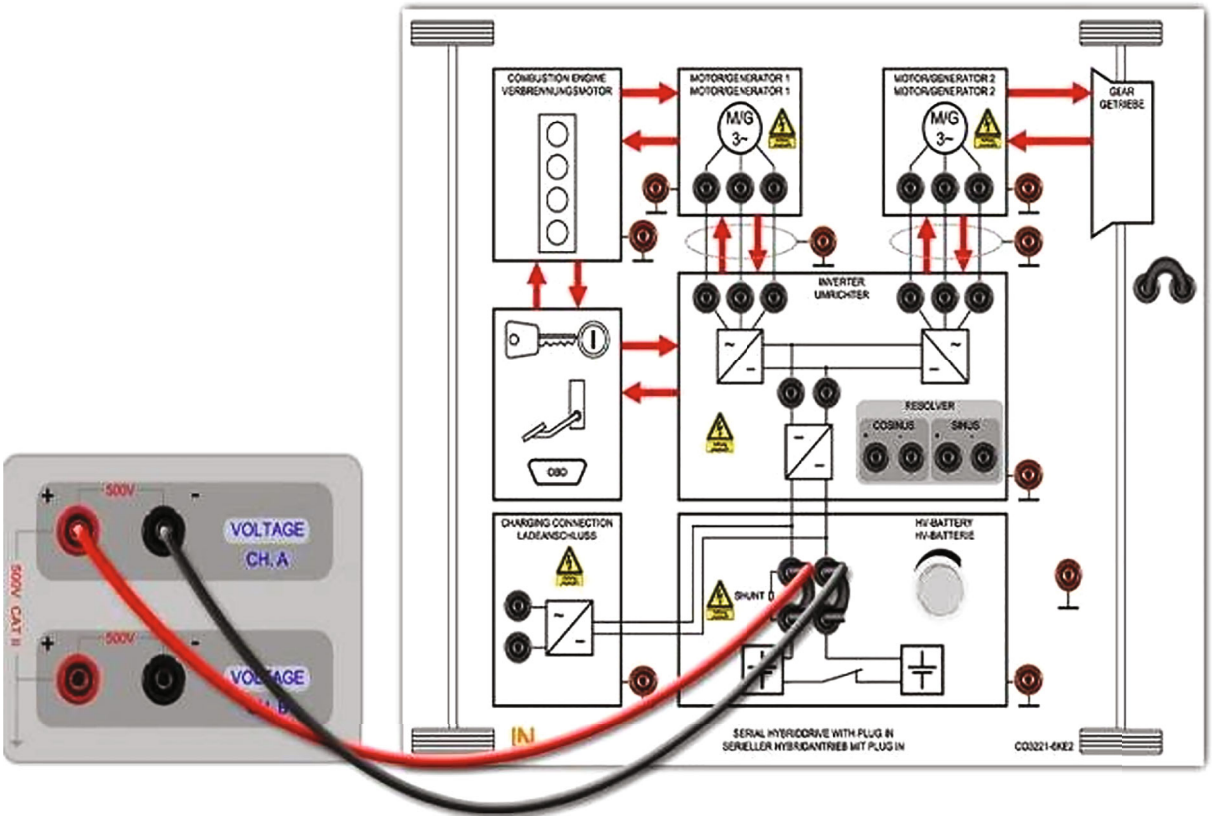

Figure 12: Didactic model of a hybrid vehicle for experimental validation.

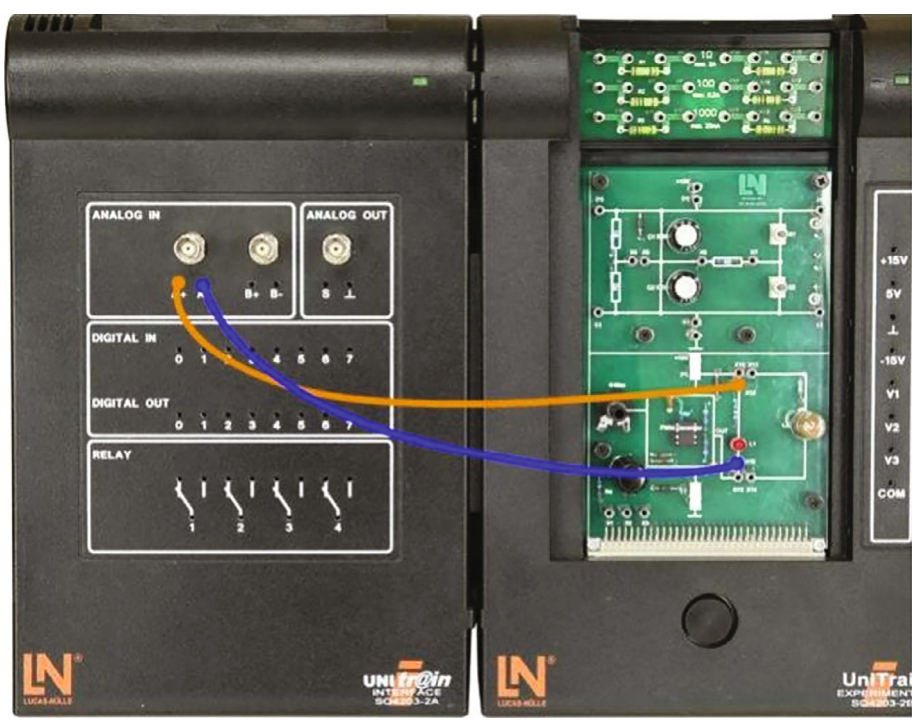

Figure 13: Proposed DC-DC model for energy harvesting device in automotive applications.

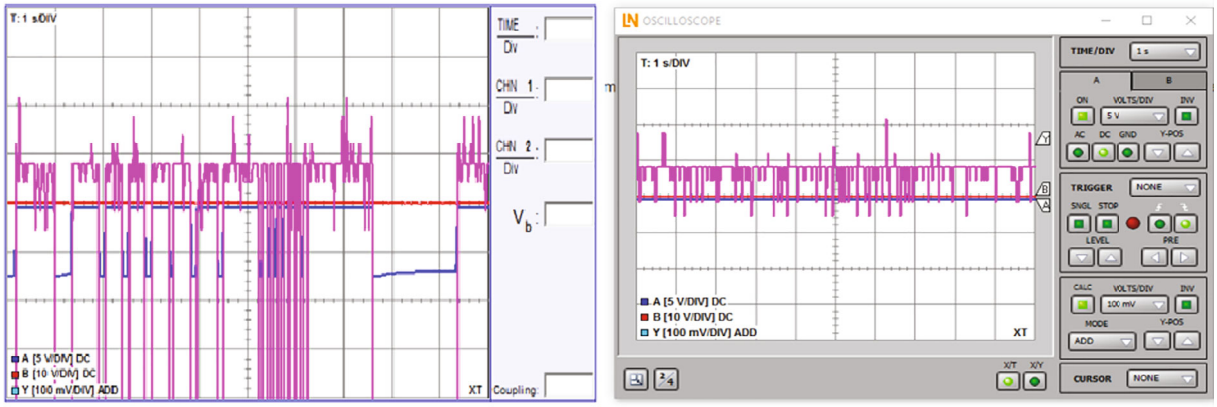

Figure 14: The harvestable electric power for the suspension system.

by a resistor as in Figure 1, the effective voltage obtained is of the order of $V_{\text{eff}} = 11.7$ V. The power is $P = 71$ mW which is higher than the previous one because the voltage has been rectified. Figure 7 illustrates the MPPT controller for the harvested power according to the changed vehicle speed. The converted power followed an exponential function of the vehicle weight amount. The harvested electric power has produced more than 90% at an unimportant interval of speed from 20 km/h to 90 km/h as highlighted in Figure 11. And outside of this range, this power production is about 20 mW. Figure 8 presents the MPPT controller for the PVEH output power.

This latter is practically continuous at the maximum value. The structure effectiveness using MPPT has been improved and reaches 90% in the occupied interval from 1 kΩ to 2.5 MΩ. The ideal value of Vpzt1 is a proportional function of the vehicle load, reaching its power optimum. Counting the nonlinear extrapolation factor, the voltage produced by the PVEH is at the ideal value with respect to the load characteristic. As the rectifier operates in the interval of optimal output value, the device can collect additional energy.

6. Conclusions

In this paper, the most MPPT algorithms used for tracking the MPP of the piezoelectric harvester system have been extensively established. Based upon the purposed algorithm, a piezoelectric harvester optimal prototype has been designed for nonlinear structures using state-dependent bond graph architecture as presented in Figures 9 and 14. The BG has exhibited the rectifier complications in PVEH schemes. We have shown that the enhanced approach eliminates the shortcomings of earlier transformers by means of an MPPT controller and a single DC-DC converter. The proposed MPPT algorithm ensured an extraction efficiency higher than 85% as shown in Figure 13. As such, the total productivity of the PVEH system has been found to be 70% using this modest and effective regulation of voltage. In this work, an adapted MPPT algorithm has been established that can overcome the incorrect response given by the conventional controller when the vehicle speed is suddenly increased. The modified MPPT has been calculated without any mathematical calculations suggesting a low-cost piezoelectric harvester system. Finally, the proposed method was appropriate to build a strong process for harvester prototypes in real physical schemes through a smaller vibration force amount.

Data Availability

All data used were included within the article.

Conflicts of Interest

The authors declare that they have no conflicts of interest.

References

[1] M. A. Hassan, M. A. A. Abdelkareem, M. M. Moheyeldein, A. Elagouz, and G. Tan, "Advanced study of tire characteristics and their influence on vehicle lateral stability and untripped rollover threshold," *Alexandria Engineering Journal*, vol. 59, no. 3, pp. 1613–1628, 2020.

[2] A. Saleem, N. Liu, H. Junjie, A. Iqbal, and M. A. Hayyat, "A novel based wind/solar electric vehicles for green and clean environment," *International Journal of Computer Electrical Engineering*, vol. 12, no. 2, pp. 93–101, 2020.

[3] F. Wen, K. Ren, Y. Lin et al., "Hysteresis controlled MPPT for piezoelectric energy harvesting," *IEICE Electronics Express*, vol. 17, no. 2, pp. 20190722–20190722, 2020.

[4] A. M. Shirahatti, "Analysis and simulation of active suspension system for full vehicle model subjected to random road profile," *International Journal of Innovative Research in Science, Engineering and Technology*, vol. 4, no. 1, pp. 18489–18502, 2015.

[5] D. Grzybek and P. Micek, "Experimental investigation on the piezoelectric energy harvester as the self-powered vibration sensor," *Journal of Theoretical and Applied Mechanics*, vol. 56, no. 3, pp. 687–699, 2018.

[6] K. Kecik and A. Mitura, "Energy recovery from a pendulum tuned mass damper with two independent harvesting sources," *International Journal of Mechanical Sciences*, vol. 174, p. 105568, 2020.

[7] G. A. Hassaan, "Car dynamics using quarter model and passive suspension, part VI: sprung- mass step response," *IOSR Journal of Computer Engineering*, vol. 17, no. 2, pp. 65–74, 2015.

[8] S. Touairi and M. Mabrouki, "Improve the energy harvesting alternatives using the bond graph approach for powering critical autonomous devices," in *International Conference on Digital Technologies and Applications*, Springer International Publishing, Cham, 2021.

[9] K. Fleurbaey, N. Omar, M. E. Baghdadi, J.-M. Timmermans, and J. V. Mierlo, "Analysis of hybrid rechargeable energy storage systems in series plug-in hybrid electric vehicles based on simulations," *EPE*, vol. 6, no. 8, pp. 195–211, 2014.

[10] X.-S. Wang and B. P. Mann, "Attractor selection in nonlinear energy harvesting using deep reinforcement learning," 2020, https://arxiv.org/abs/2010.01255.

[11] S. Ertarla, C. V. Karadag, and N. Topaloglu, "Axial and transverse vibration of a cantilever beam energy harvester with a tip mass with axial and transverse eccentricity," in *Proceedings of the 14th International Conference on Vibration Problems*, pp. 943–955, Springer Singapore, 2021.

[12] R. Queiroz, D. Sharma, R. Caldas et al., "A driver-vehicle model for ADS scenario-based testing," https://arxiv.org/abs/2205.02911.

[13] S. Hardman, A. Jenn, G. Tal et al., "A review of consumer preferences of and interactions with electric vehicle charging infrastructure," *Transportation Research Part D: Transport and Environment*, vol. 62, pp. 508–523, 2018.

[14] M. Peng, L. Liu, and C. Jiang, "A review on the economic dispatch and risk management of the large-scale plug-in electric vehicles (PHEVs)-penetrated power systems," *Renewable and Sustainable Energy Reviews*, vol. 16, no. 3, pp. 1508–1515, 2012.

[15] I. J. Tiemessen, C. T. J. Hulshof, and M. H. W. Frings-Dresen, "An overview of strategies to reduce whole-body vibration exposure on drivers: a systematic review," *International Journal of Industrial Ergonomics*, vol. 37, no. 3, pp. 245–256, 2007.

[16] W. J. Smith, "Can EV (electric vehicles) address Ireland's CO_2 emissions from transport?," *Energy*, vol. 35, no. 12, pp. 4514–4521, 2010.

[17] K. Hedegaard, H. Ravn, N. Juul, and P. Meibom, "Effects of electric vehicles on power systems in Northern Europe," *Energy*, vol. 48, no. 1, pp. 356–368, 2012.

[18] M. Mahmoud, R. Garnett, M. Ferguson, and P. Kanaroglou, "Electric buses: a review of alternative powertrains," *Renewable and Sustainable Energy Reviews*, vol. 62, pp. 673–684, 2016.

[19] A. Harb, "Energy harvesting: state-of-the-art," *Renewable Energy*, vol. 36, no. 10, pp. 2641–2654, 2011.

[20] P. Fabianek, C. Will, S. Wolff, and R. Madlener, "Green and regional? A multi-criteria assessment framework for the provision of green electricity for electric vehicles in Germany," *Transportation Research Part D: Transport and Environment*, vol. 87, article 102504, 2020.

[21] A. E. Kazdin, "Improving the quality of care and reducing the burden of clinical dysfunction," *Administration and Policy in Mental Health*, vol. 37, no. 1-2, pp. 160–166, 2010.

[22] X. Zhang and X. Bai, "Incentive policies from 2006 to 2016 and new energy vehicle adoption in 2010–2020 in China," *Renewable and Sustainable Energy Reviews*, vol. 70, pp. 24–43, 2017.

[23] M.-G. Kang, W.-S. Jung, C.-Y. Kang, and S.-J. Yoon, "Recent progress on PZT based piezoelectric energy harvesting technologies," *Actuators*, vol. 5, no. 1, 2016.

[24] G. Yakubu, G. Sani, S. B. Abdulkadir, A. A. Jimoh, and M. Francis, "Full car active damping system for vibration control," *International Journal of Engineering Technologies and Management Research*, vol. 6, no. 4, pp. 1–17, 2020.

[25] A. Aldair and E. Alsaedee, "Regeneration energy for nonlinear active suspension system using electromagnetic actuator," *Iranian Journal of Electrical and Electronic Engineering*, vol. 16, no. 2, pp. 113–125, 2020.

[26] R. Tavares and M. Ruderman, "Energy harvesting using piezoelectric transducers for suspension systems," *Mechatronics*, vol. 65, article 102294, 2020.

[27] A. Hegendörfer, P. Steinmann, and J. Mergheim, "Investigation of a nonlinear piezoelectric energy harvester with advanced electric circuits with the finite element method," *SN Applied Sciences*, vol. 4, no. 4, p. 120, 2022.

[28] A. Heidarian and X. Wang, "Review on seat suspension system technology development," *Applied Sciences*, vol. 9, no. 14, p. 2834, 2019.

[29] N. Kumar, B. Singh, J. Wang, and B. K. Panigrahi, "A framework of L-HC and AM-MKF for accurate harmonic supportive control schemes," *IEEE Transactions on Circuits and Systems I*, vol. 67, no. 12, pp. 5246–5256, 2020.

[30] E. Kurt, D. Özhan, N. Bizon, and J. M. Lopez-Guede, "Design and implementation of a maximum power point tracking system for a piezoelectric wind energy harvester generating high harmonicity," *Sustainability*, vol. 13, no. 14, p. 7709, 2021.

[31] N. Kumar, B. Singh, and B. K. Panigrahi, "Integration of solar PV with low-voltage weak grid system: using maximize-M Kalman filter and self-tuned P&O algorithm," *IEEE Transactions on Industrial Electronics*, vol. 66, no. 11, pp. 9013–9022, 2019.

[32] T. Darabseh, D. Al-Yafeai, A. I. Mourad, and F. Almaskari, "Piezoelectric method-based harvested energy evaluation from car suspension system: simulation and experimental study," *Energy Science & Engineering*, vol. 9, no. 3, pp. 417–433, 2021.

[33] T. Tan, Z. Wang, L. Zhang, W.-H. Liao, and Z. Yan, "Piezoelectric autoparametric vibration energy harvesting with chaos control feature," *Mechanical Systems and Signal Processing*, vol. 161, p. 107989, 2021.

[34] K. Fan, S. Liu, H. Liu, Y. Zhu, W. Wang, and D. Zhang, "Scavenging energy from ultra-low frequency mechanical excitations through a bi-directional hybrid energy harvester," *Applied Energy*, vol. 216, pp. 8–20, 2018.

[35] S. Touairi and M. Mabrouki, "Control and modelling evaluation of a piezoelectric harvester system," *International Journal of Dynamics and Control*, vol. 9, pp. 1559–1575, 2021.

[36] S. Touairi and M. Mabrouki, "Vibration harvesting integrated into vehicle suspension and bodywork," *Indonesian Journal of Electrical Engineering and Computer Science*, vol. 23, no. 1, p. 188, 2021.

[37] S. Touairi and M. Mabrouki, "Chaotic dynamics applied to piezoelectric harvester energy prediction with time delay," *International Journal of Dynamics and Control*, vol. 10, pp. 699–720, 2021.

[38] S. Touairi, A. Bouzid, and M. Mabrouki, "Road handling of regenerative motorcycle suspensions and energy harvesting," *AIP Conference Proceedings*, vol. 2345, article 020017, 2021.

[39] S. Touairi and M. Mabrouki, "Optimization of harvester system in embedded vehicle systems via bond graph modeling algorithm," in *2020 IEEE 6th international conference on optimization and applications (ICOA)*, pp. 1–6, Beni Mellal, Morocco, 2020.

[40] S. Touairi and M. Mabrouki, "Optimization of energy harvesting system design by functional analysis," in *2020 1st International Conference on Innovative Research in Applied Science, Engineering and Technology (IRASET)*, pp. 1–6, Meknes, Morocco, Apr. 2020.

[41] G. Na, H. Lee, and Y. Eun, "A multiplicative coordinated stealthy attack for nonlinear cyber-physical systems with homogeneous property," *Mathematical Problems in Engineering*, vol. 2019, Article ID 7280474, 13 pages, 2019.

[42] N. Kumar, B. Singh, B. K. Panigrahi, C. Chakraborty, H. M. Suryawanshi, and V. Verma, "Integration of solar PV with low-voltage weak grid system: using normalized Laplacian kernel adaptive Kalman filter and learning based InC algorithm," *IEEE Transactions on Power Electronics*, vol. 34, no. 11, pp. 10746–10758, 2019.

[43] N. Kumar, B. Singh, B. K. Panigrahi, and L. Xu, "Leaky-least-logarithmic-absolute-difference-based control algorithm and learning-based InC MPPT technique for grid-integrated PV system," *IEEE Transactions on Industrial Electronics*, vol. 66, no. 11, pp. 9003–9012, 2019.

[44] N. Kumar, B. Singh, and B. K. Panigrahi, "LLMLF-based control approach and LPO MPPT technique for improving performance of a multifunctional three-phase two-stage grid integrated PV system," *IEEE Transactions on Sustainable Energy*, vol. 11, no. 1, pp. 371–380, 2020.

[45] A. Brenes, A. Morel, J. Juillard, E. Lefeuvre, and A. Badel, "Maximum power point of piezoelectric energy harvesters: a review of optimality condition for electrical tuning," *Smart Materials and Structures*, vol. 29, no. 3, article 033001, 2020.

[46] H. Karmouni, M. Chouiekh, S. Motahhir et al., "A novel MPPT algorithm based on Aquila optimizer under PSC and implementation using raspberry," in *2022 11th International Conference on Renewable Energy Research and Application (ICRERA)*, pp. 446–451, Istanbul, Turkey, 2022, September.

[47] A. El-Ghajghaj, N. E. Ouanjli, H. Karmouni, M. O. Jamil, H. Qjidaa, and M. Sayyouri, "An improved MPPT based on maximum area method for PV system operating under fast varying of solar irradiation," in *Digital Technologies and Applications: Proceedings of ICDTA'22, Fez, Morocco, Volume 1*, pp. 545–553, Springer International Publishing, Cham, 2022.

[48] M. Chouiekh, H. Karmouni, A. Lilane, K. Benkirane, D. Saifaoui, and M. Abid, "Control of a photovoltaic pumping system using the ABC algorithm in EL Jadida climate," *Technology and Economics of Smart Grids and Sustainable Energy*, vol. 7, no. 1, p. 15, 2022.

[49] H. Karmouni, M. Chouiekh, S. Motahhir, H. Qjidaa, M. O. Jamil, and M. Sayyouri, "Optimization and implementation of a photovoltaic pumping system using the sine–cosine algorithm," *Engineering Applications of Artificial Intelligence*, vol. 114, article 105104, 2022.

[50] H. Karmouni, M. Chouiekh, S. Motahhir, H. Qjidaa, M. O. Jamil, and M. Sayyouri, "A fast and accurate sine-cosine MPPT algorithm under partial shading with implementation using Arduino board," *Cleaner Engineering and Technology*, vol. 9, article 100535, 2022.

[51] B. N. Nguyen, V. T. Nguyen, M. Q. Duong, K. H. Le, H. H. Nguyen, and A. T. Doan, "Propose a MPPT algorithm based on Thevenin equivalent circuit for improving photovoltaic system operation," *Frontiers in Energy Research*, vol. 8, article 474640, 2020.